ELSEVIER

Image and Vision Computing 19 (2001) 891–911

image AND vision COMPUTING

www.elsevier.com/locate/imavis

Gaze determination via images of irises

Jian-Gang Wang[a], Eric Sung[b,*]

[a]*Center for Signal Processing, School of Electrical and Electronic Engineering, Nanyang Technological University, Nanyang Avenue, Singapore, Singapore 639798*

[b]*Division of Control and Instrumentation, School of Electrical and Electronic Engineering, Nanyang Technological University, Nanyang Avenue, Singapore, Singapore 639798*

Received 11 May 2000; revised 20 December 2000; accepted 21 January 2001

Abstract

In this paper, we present a new approach for measuring eye-gaze of human via images of the irises. Two iris contours are approximately modeled as two circles having known radii and we estimate the ellipses of their projections onto image plane, respectively. The eye-gaze, defined in this paper as the unit surface normal to the supporting plane of the iris, can be estimated from the projection of the iris contour (limbus). The unique solution of the eye-gaze was obtained based on a geometric constraint, namely that the difference between the two normal directions to the supporting planes of the left and right iris should be minimal, irrespective of eyeball rotations and head movements. Furthermore, the 3D location of the center of the irises can be calculated if the radius of the iris contour is given. The robustness of this approach was verified by experiments on synthetic and real image data.

In order to obtain a higher resolution of the iris, a zoom-in camera is used. This creates an additional problem of having to relate the camera for estimating the head-pose to the iris camera. A general approach that combines head-pose determination with gaze estimation is proposed.

Keywords: Gaze determination; Iris contour; Circle/ellipse; Model-based monocular vision; Focus point; Human–machine interaction

1. Introduction

Increasing computing power has allowed many new concepts of man–machine interaction to be realized. Vision-based approach, for example, is a more natural and an intuitive user interface than those using devices such as mouse, data glove and helmet. With the new interface, one can operate the computer without requiring the human operator to acquire specialized training. It can also free the human from having to wear tedious equipment such as a head-mounted camera used in virtual reality [1,22]. Measuring head-pose and eye-gaze for human–machine/robot interaction has been investigated in some previous researches [9,18,20]. Computer vision techniques specifically developed for hard real-time robotic applications are certainly adequate for interaction applications, because such techniques often rely on simplified linear models of camera–world interaction in order to dramatically reduce the burden of visual computations (see recent work by Cipolla and Hollinghurst [31], Allotta and Colombo [32]).

Our interest in this paper was originally motivated with consideration of how to interact with a computer using head-pose and eye-gaze that measured from images of head and eyes rather than having extra measurement devices such as helmet and infrared-light emitting diode (LED). The research is important because, despite the recent research and technological efforts, advanced human–computer interaction devices still suffer from a number of problems, if not solved, are likely to hamper the widespread diffusion of the next generation computer interfaces. Two major problems with the current device are *intrusiveness* (e.g. wearing a virtual reality helmet is not exactly fun) and *expansiveness* (related to the need of special hardware and high computational overload).

There are two components to gaze orientation: pose of human head and the orientation of the eye within their sockets. We have investigated these two aspects and will concentrate on the second part in this paper. However, 3D location of the iris contour can be determined besides the gaze orientation in our eye-gaze determination algorithm. The contours of the two irises (not the irises) are assumed circles having known radii in space and a method to determine the gaze of a person by using the person's contours of the irises is demonstrated in this paper. We define the gaze as the normal direction to the supporting plane of the iris. The actual gaze direction is measured by kappa (κ), which is the angle between the visual axis and the anatomical axis of

* Corresponding author. Tel.: +65-790-5419; fax: +65-792-0415.
E-mail address: eericsung@ntu.edu.sg (E. Sung).

0262-8856/01/$ - see front matter
PII: S0262-8856(01)00051-8

the eye. Because our defined gaze direction is almost a fixed relation with κ, it does not really matter which one is used. However, for practical purposes, our definition will be the one to be adopted.

There are two solutions of the normal to the supporting plane of the iris contour and its center from the projection of the iris. The prior knowledge of the eye model has been utilized to disambiguate the solutions in our method, namely that the difference between the two normal directions to the supporting planes of the two irises should be minimal, irrespective of eyeball rotations and head movements. We call this constraint the 'normal direction constraint'.

The gaze vectors of the two eyes are parallel when a person focuses at infinity. We make the assumption that the person is not looking at too close an object. However, if he is looking at objects of at least one meter away, the eyes gaze vectors of the two eyes are quite parallel. We disambiguate the solution by selecting the two normal pairs that are close to each other.

The projections of the contours of the two irises are fitted as ellipses, this is true also due to the shape of the eye. Eye is not a sphere. The anterior–posterior diameter (front-to-back) is largest, but the horizontal diameter is also larger than the vertical diameter. In most existing approaches, the iris contours on the image plane are assumed to be circles, so the felicitous circular geometry is utilized and iris outer boundaries (limbus) are detected using circle edge operator. We can verify the correctness of our elliptical assumption from the eccentricity of the iris contours found experimentally.

From the observed perspective projection of a circle having known radius, it is possible to infer analytically the supporting plane of the circle, as well as the center of the circle [8]. The problem has been extensively investigated and there are many papers concentrating on 3D location of circular objects [6,8,12,14,23–25,28,29]. A method is presented in Ref. [23] to determine the pose from circles exploiting the property that the back-projected curve must have equal coefficients for X^2 and Y^2 and no XY term. Ji et al. [24] proposed an algebraic solution using a similar way. However, the solution of the unit surface normal to the supporting plane of the circle is not unique. We have successfully developed a 'two-circles' pose determination method [17,36] using a monocular view of two coplanar circles with known radii. In this paper, we develop it further for human gaze determination in conjunction with two iris contours. We noticed that the difference of the normal to the supporting plane of iris contours and 'normal direction constraints' is applied. The simulation on synthetic data showed that our 'two-circles' algorithm is robust to image noise and has satisfactory accuracy.

Facial features, such as the eye- and mouth-corners, the tip of the nose, ratios of the distances between the feature points, can be utilized to determine either the head-pose [15,18] or eye-gaze [7]. More compact features, such as eye contours, can be utilized to improve the measurement 'robustness'. For instance, affine deformations to the contours of the two eyes are used to estimate the head displacement in Ref. [20]. A technique was presented to infer the computer screen location currently observed by the user from the measurement of image of the eye pupil displacements [3]. Head tracking and pupil detection are obtained by coupling an elastic template with the raw image data. The template models the external eye contour with elliptic arcs while modelling the iris with an ellipse, whose center locates the pupil. In Refs. [9,22], eyes are tracked for human–computer interaction by installing an infrared camera, provided with a transmitter and receiver. It evaluates the current pupil position by exploiting the differences in infrared reflection between the pupil and the surrounding iris and sclera. However, the system's calibration is sensitive to the movement of the subject's head, so the subject must either remain perfectly still or wear a cumbersome headgear to maintain a constant separation between the sensor and the eye. Gee et al. [7] did not consider the eyeball's rotation in their gaze estimation approach because they noticed the low resolution of the eye image. They estimate the gaze direction by using the baseline of the eyes. Colombo et al. [27] models the visible eyeball portions of the user's eye-balls as planar surfaces, and regard any gaze shift related to an eyeball rotation as a translation of the pupil in the face plane.

The iris, feature used in our gaze determination approach, is prominent and reliable facial feature within the eye region. The special character of the iris structure, namely the transition from white-to-dark then dark-to-white, makes it possible to segment iris from eye region reliably. However, detection of the human eye is often a very difficult task when the contrast of the eye is very poor. The method that uses deformable template, such as Yuille et al. [21], Xie et al. [10] and Lam et al. [19], is a popular method in locating the human eye. However, it is feasible only if the initial position of the eye model is estimated near enough to the actual eye position. Moreover, this deformable model is computationally expensive and is required to determine the weight factors for certain energy terms manually. An improved method was proposed by Deng et al. [11], which combines deformable templates and an edge operator to do eye-feature extraction, description and tracking. An extended iris mask was used to select iris edge from Canny edge operator results that are still very noisy even in a clear image. The faces must be nearly frontal-view and the image of the eyes should be large enough to be described by the template. Lam et al. [19] developed a method to detect eye features from face images using salient corner features. Daugman [16] located an iris by using Integro-differential operators where the felicitous circular geometry of the iris is exploited. In Ref. [5], the model knowledge and context are used to help detecting iris. The left edge segment (vertical, bright-to-dark edge) of the iris is detected using a 'basis filter' while the corresponding right edge is subsequently searched using the model knowledge and the size, position and orientation of the left edge segment. In order to

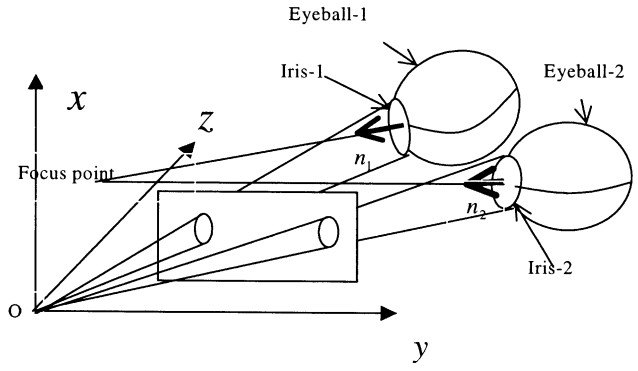

(a)

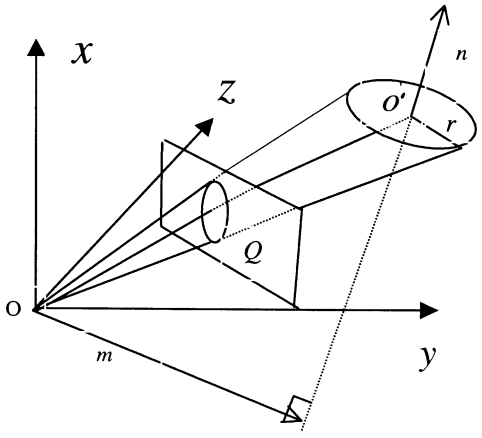

(b)

Fig. 1. The projection of a circle and the rotation axis of the circle.

speed up the measurement, the pupil is always modeled as a circle although it should in general be elliptical [4].

In this paper, the eye regions are located using our head-pose determination algorithm [26,36]. Next, the special characteristic of iris intensity image, namely the transition from white-to-dark then dark-to-white, is used to detect the iris. The iris is partially occluded by the upper and lower eye lids so it is difficult to fit the ellipse accurately. A zoom-in camera, gaze-camera, is used in order to improve the resolution of the iris image. The problem of having possible out-of-field views can be settled by guiding the gaze-camera using the head-pose information obtained by pose-camera.

Compared with other approaches, we can estimate the gaze without considering the compensation of the head movement. This is because the gaze we defined can be located uniquely in the coordinate system of the camera, irrespective of movements of the 'eyeball's center' (due to the head movement). We do not require the sphere to be a sphere. Most conventional systems simply ignore the changes of gaze vectors due to head movement by limiting the range of head movement and keeping the measuring errors smaller than the variation caused by the change of fixation points. The research about compensation of the human head movement can be found in Ref. [4], where the compensation must be considered because the eye is assumed to be a sphere and the 'center of the eyeball' is defined as the starting point of the gaze vector. The eye-gaze will alter when the gaze of the direction fixes on the same point and the center of the eyeball changes (by movement of the head). A dynamic model is introduced in Ref. [4] which distinguishes between the changes of gaze vectors due to head movement and due to the varied gaze direction, and compensates the head movement.

Iris detection is described in Section 2.1; 'two-circles' positioning algorithm is discussed in Sections 2.2. Eye model and the experiment results are discussed in Section 3. And finally, the conclusion is given in Section 4.

2. Positioning

The perspective projection of a circle on image plane is an ellipse. With the two iris contours, it will be shown that the two respective equations lead to a unique solution of the eye-gaze.

2.1. Iris detecting

The most prominent and reliable features within the eye region are edges of the iris. Because we wish to model iris contour as an ellipse on the image plane, obviously the existing iris detection methods using circular edge operators cannot be used. Instead, we detect the iris edge (bright-to-dark and dark-to-bright step edge) using a (3×3) vertical edge operator and morphological 'open' operations. The iris can be segmented using a threshold that is selected by analyzing histogram of the eye region. Then, the ambiguous parts connecting the iris region, caused by the dark points that lie on the eyelids or the eye-corner, can be separated from the iris using morphological 'open' operation, with a 2×2 structuring element. Then a vertical edge operator is used to detect the iris edges. The eyelids generally obscure the upper and lower limbus of the iris, so we can fit the iris contours using the visible edges of the iris.

The high contrast between iris and the eye white makes the iris edges to be located reliably. Once the iris edges are obtained, iris contour is fitted to an ellipse. Fitting elliptical sections to data is a notoriously ill-conditioned problem. The problems are due to the spread of points, a small elliptical arc length and knowing exactly which points in the image lie on the ellipse. A review of ellipse fittings can be found in Ref. [35]. We fit the contour of the iris using the method proposed by Porrill [13]. We adopt Porill's algorithm, a Kalman filter approach, because it naturally includes prior information about the ellipse and eliminates the curvature bias associated with the Bookstein algorithm

[34]. We have found that accurate fitting results can be obtained although only partial edges can be seen on the iris contours. It is stable to detect an ellipse even under the condition when the iris moves to one extreme side of the eye.

2.2. 'Two-circles' algorithm

In this paper, eye-gaze is defined as the unit surface normal (passing the iris's center) to the supporting plane of the iris. Our definition of 'eye-gaze' is obviously an adequate representation of the human's focus of interest. It has a fixed relationship with the anatomical axis of the eye (Section 3.1.1). We model the contour of the iris as a circle having known radius, so the gaze can be determined by estimating the projection of the iris contour. The disadvantage of using circles is that there is a two-fold ambiguity in the recovered plane. We will show that the solutions can be disambiguated using the image of the contours of the two iris — 'two circles' algorithm.

We determine the normal direction of each iris contour, respectively, using a vector algebraic method as detailed below. Then the unique solution of the gaze can be obtained from each contour's two ambiguous solutions by applying 'the normal direction constraint'. Once the gaze is determined, the 3D centers of two iris contours can be determined.

2.2.1. Pose from contour of iris

The projection of contours of the two irises is shown in Fig. 1(a), where the eye-gaze is represented as n_1 and n_2.

The spatial relation between a circle and its perspective on the image plane is shown in Fig. 1(b). The camera coordinate system is *O-XYZ*, the circle's center is O' and the radius is r. Let n be the unit normal to the supporting plane of the circle.

Herein, we will describe briefly the algorithm for determining the pose from a circle and its projection [2,17,23,29]. A method for estimating eye-gaze based on the 'normal direction constraint' is then presented.

For convenient representation, image coordinate (x', y') are initially normalized using following formulas:

$$x = \frac{x' - x_0}{f_x} \tag{1}$$

$$y = \frac{y' - y_0}{f_y} \tag{2}$$

where (x_0, y_0) are coordinates of the image-center point (principal point), f_x and f_y are the scale factors of the camera along the *X*- and *Y*-axis, respectively. Using the normalized camera, i.e. the image plane is located at a unit distance from the optical center (focal length $f = 1$), we have

$$X_i = x_i Z_i \tag{3}$$

$$Y_i = y_i Z_i \tag{4}$$

where (X_i, Y_i, Z_i) is the coordinate of a point under the camera coordinate system, (x_i, y_i) is the corresponding image coordinate of the point. We get two solutions of the normal to the supporting plane of the iris and consequently two solutions of the iris's center from its projection using the approach described as follows.

Let ellipse $\mathbf{Q}$ (nonzero real symmetric matrix in the quadratic form representation) represent a projection of a circle of radius r under the normalized camera coordinate system. λ_1, λ_2 and λ_3 be the eigenvalues of $\mathbf{Q}$ ($\lambda_3 < 0 < \lambda_1 \leq \lambda_2$), and u_1, u_2 and u_3 are the unit eigenvectors for eigenvalues λ_1, λ_2 and λ_3, respectively. The normal to the supporting plane will be ([2,17,23,29]):

$$n = u_2 \sin\theta + u_3 \cos\theta \tag{5}$$

where

$$\sin\theta = \sqrt{\frac{\lambda_2 - \lambda_1}{\lambda_2 - \lambda_3}} \tag{6}$$

$$\cos\theta = \sqrt{\frac{\lambda_1 - \lambda_3}{\lambda_2 - \lambda_3}} \tag{7}$$

The vector that starts from the viewpoint and orthogonal to the normal n (see Fig. 1(b)) is:

$$m = u_2 \cos\theta - u_3 \sin\theta \tag{8}$$

The centers of the iris contour in space can be determined using Eqs. (5) and (8) and radius r.

Note that the signs of the eigenvectors u_1, u_2 and u_3 are arbitrary. Since n and $-n$ indicate the same surface orientation, the number of 3D interpretations is as follows:

1. if $\lambda_1 \neq \lambda_2$, two interpretations exist;
2. if $\lambda_1 = \lambda_2$, only one interpretation exists.

The second case, when one interpretation exists, will happen only when the optical axis is parallel to the normal to the supporting plane of a circle and passes through the center of the circle. Hence, we cannot expect to have only one interpretation independently from the two irises in a face image. In other words, in an image of two irises, if there exists only one solution from the contour of any iris, then there will be two solutions from the contour of another iris.

2.2.2. Normal direction constraint

In Section 2.2.1, we can see that we generally have two ambiguous 3D interpretations from a couple of circle–ellipse correspondent. We need to disambiguate the solutions using other constraint in our gaze determination approach.

Assuming two iris contours are fitted [13] on the image plane, respectively, resulting Q_1 and Q_2, see Fig. 1. Hence, the 3D location of the two iris contours can be determined using the circle–ellipse correspondent, respectively. We propose the 'normal direction constraint' to disambiguate the normal solutions. Totally four normal directions can be obtained from the two irises, two for the left iris and two for the right iris. In general, the eye-gazes of the two eyes meet

at a point of interest. The eye-gazes of the two eyes are parallel when the person focuses at infinite. When the distance is not great, there is possibly a noticeable angle between the two eye-gaze vectors. Our 'normal direction constraint' disambiguates the normal solutions by searching the gaze of the two eyes, which have minimal difference.

Consider the two solutions of the normal and center to Q_1 as (n_{11}, O_{11}) and (n_{12}, O_{12}), where n_{11} and n_{12} represent the normal to Q_1, O_{11} and O_{12} are the corresponding centers of Q_1. Similarly, consider the two solutions to Q_2 as (n_{21}, O_{21}) and (n_{22}, O_{22}). We represent the angle between n_{11} and n_{21}, n_{11} and n_{22}, n_{12} and n_{21}, n_{12} and n_{22} as $\angle(n_{11}, n_{21})$, $\angle(n_{11}, n_{22})$, $\angle(n_{12}, n_{21})$ and $\angle(n_{12}, n_{22})$ respectively.

We consider two normal directions in which the difference is minimal. In other words, the angle between one of the normal directions to the supporting plane of the left iris and one of the normal directions of the right plane is minimal among the angles formed by all possible couples of normal, one from left iris and one from right iris.

When the focus point is at infinity, the gaze of the two eyes is parallel, i.e. the difference between the gaze of the two eyes is zero, the other two normal directions is not zero, so the 'normal direction constraint' is obviously right. When the distance is great (1 m for example), the gaze of the two eyes is nearly parallel because the distance between the two eyes can be neglected with respect to the focus distance. The difference between the gaze of the two eyes is far smaller than the difference of the redundant normal solutions. The 'normal direction constraint' is right. There is a noticeable angle between the gaze of the two eyes when the distance is not great (0.5 m for example). However, 'normal direction constraint' is right because we cannot expect an abrupt change of the differences we are considering. In our experiments, we found that the difference of the redundant normal is at least three times the difference of the gaze of the two eyes when the distance is 0.5 m.

The procedure of the 'normal direction constraint' can be described as follows.

```
Begin
{
If ∠(n11, n21) = min(∠(n11, n21), ∠(n11, n22), ∠(n12, n21) ∠
(n12, n22))
{
   the unique solution of the left iris is: (n11, O11);
   the unique solution of the right iris is: (n21, O21)
}
else if ∠(n11, n22) = min(∠(n11, n21), ∠(n11, n22), ∠(n12,
n21) ∠(n12, n22))
{
   the unique solution of the left iris is: (n11, O11);
   the unique solution of the right iris is: (n22, O22)
}
else if ∠(n12, n21) = min(∠(n11, n21), ∠(n11, n22), ∠(n12,
n21) ∠(n12, n22))
{
   the unique solution of the left iris is: (n12, O12);
   the unique solution of the right iris is: (n21, O21)
}
else
{
   the unique solution of the left iris is: (n12, O12);
   the unique solution of the right iris is: (n22, O22)
}
}
End
```

The computing of the 'two-circles' algorithm is light. The accuracy of the algorithm is high, thanks to the high-resolution images of the irises. The eye edges can be located because the contrast of the eye-black and eye-white. There are more points for fitting contour of the iris although irises are partially occluded by the eyelids. The 'normal direction constraint' can disambiguate the gaze solution robustly. This can be seen from the following experiments.

3. Experimental investigation and results

We have tested our gaze determination method using a Pentium450 PC, 128MB RAM. The algorithm runs on Image-Pro Plus image processing software with Matrox Meteor-II imaging board. The pose camera (Model name: HUNT, HTC 460) is mounted on a fixed tripod while the gaze camera is mounted on a computer controlled pan-tilt unit (PTU-46-17.5, see Fig. 2(b)). The focal length of the gaze camera can be adjusted from 5.4 to 64.8 mm. The distance between the gaze camera and the operator is about 1 m. Our head-pose and eye-gaze estimation system is shown in Fig. 2(a), where the right camera is a head-pose camera and the left one is the gaze camera.

The experiments include simulation using synthetic data and real scene and is described now.

3.1. Simulations on exact data

In order to understand the accuracy of the proposed algorithm, a model of the human eye is used in our simulations.

3.1.1. Eye model

The eye is like a fine camera, with a shutter, iris, and lens system on one side and a sensitive film called retina on the other. In contrast to the conventional camera, where focusing is accomplished by moving the lens, the cornea and the lens of the eye remain fixed and the focal length is changed by bending of the lens by the eye muscles. The eye muscles are most relaxed when the eye is looking at distant objects (i.e. 'focused at infinite'), so that many optical calculations involving the eye are made under that assumption. Human eyes are very nearly spherical in shape except for a bulge at the front. They are about an inch in diameter. The front-to-back diameter (anteroposterior diameter) of the eye is largest, the horizontal diameter is greater than the vertical

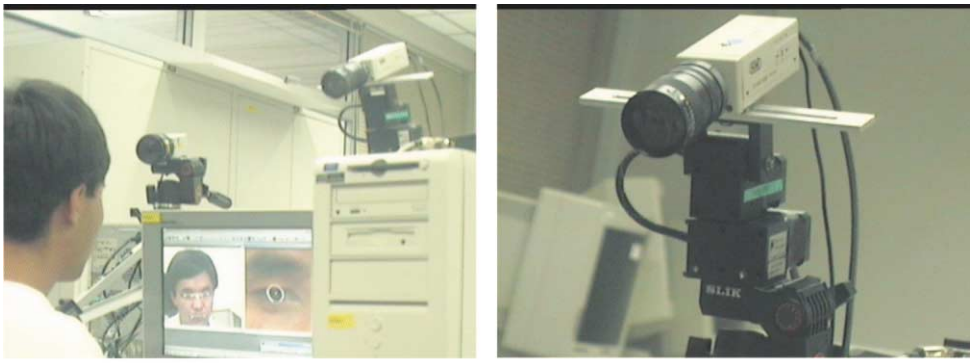

(a) (b)

Fig. 2. Integration of head-pose and eye-gaze, (a) left: pose camera, right: gaze camera, (b) pan-tilt unit.

diameter. The front portion is somewhat more sharply curved, and is covered by a tough, transparent membrane, called the cornea. The region behind the cornea contains a liquid, called the aqueous humor. Next comes the crystalline lens. The diameter of the eyeball is about 25 mm, and the radius of the iris is about 7 mm. Gullstrand gave some of the pertinent facts for a normal human eye [30]. Gullstrand's schematic eye is shown in Fig. 3.

The human eye can be moved because the back of them is approximately spherical and is situated in an approximately spherical socket. They can be rotated rapidly within the sockets by the action of six strong, precisely controlled extraocular muscles. Our algorithm made minimum assumption on the eye model. We do not need to know the eyeball in shape. Only the visible iris edges of the human eye are utilized in our approach. The iris contours (not the irises) are modelled as two circles and eye-gaze can be estimated using their projection (two ellipses) on an image plane. The normal to the supporting plane of the iris contours is defined as the gaze vector. The eye-gaze we defined passes through the pupil's and eyeball's center. It keeps a near fixed angle (κ, the angle between the visual and the anatomical axis of the eye) with the central gaze vector that is determined by the eye lens. It is only a matter of calibration relationship between our gaze and the central gaze vector.

Our definition of the gaze is obviously an adequate gaze, this can be observed in our daily life.

A simplified model is defined (see Fig. 4). The iris is located at the front of eyeball and its contour is modeled as a circular ring of radius r (see Fig. 4(a)).

The upper and lower eyelids are modeled as two parabolas (Fig. 4 (b)). The upper eyelid passing through points $P_1(x_1, y_1)$, $P_2(x_2, y_2)$ and $P_3(x_3, y_3)$, the lower eyelid passing through points $P_1(x_1, y_1)$, $P_4(x_4, y_4)$ and $P_3(x_3, y_3)$. The equation of the eyelid is:

$$y = a(x - b)^2 + c \tag{9}$$

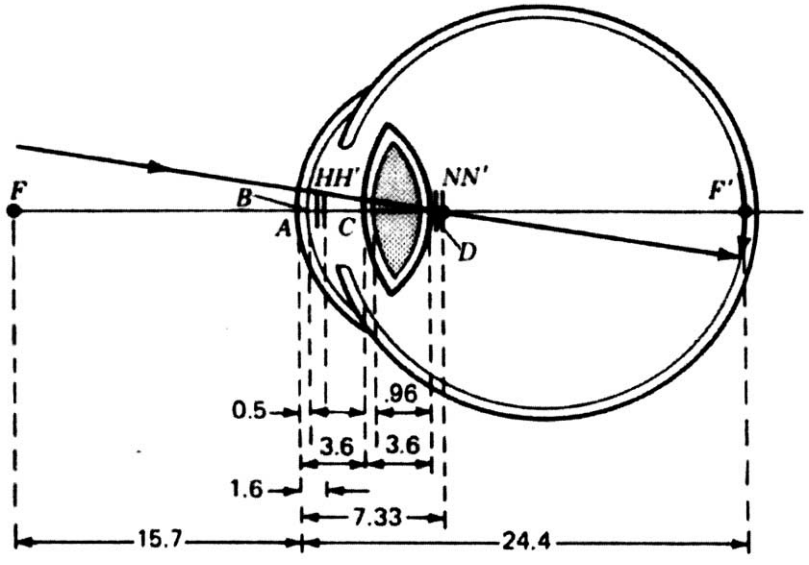

Fig. 3. Schematic eye as developed by Gullstrand, showing the real and inverted image on the retina (dimensions are in millimeters).

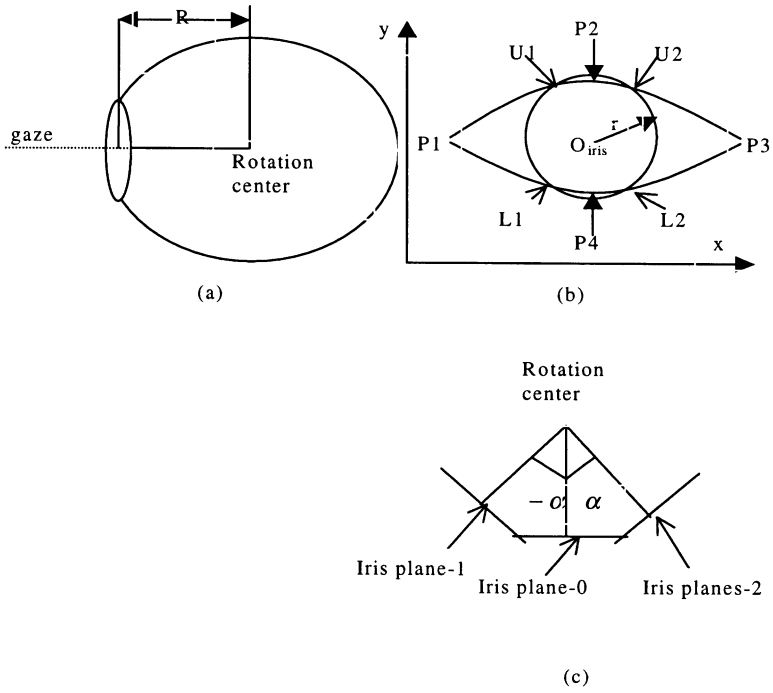

Fig. 4. The eye model, (a) The eyeball, the iris and the gaze, (b) the coordinate system, upper and lower eyelids, the radius of the iris, (c) the rotation of the iris about the center of the eyeball, 'iris plane-1' and 'iris plane-2' are formed by rotating the initial 'iris plane-0' about the center of the eyeball α and $-\alpha$ respectively.

which for the upper eyelid yields:

$$a = \frac{-y_2}{(x_1 - x_2)^2} \tag{10}$$

$$b = x_2 \tag{11}$$

$$c = y_2 \tag{12}$$

while for the lower eyelid yields:

$$a = \frac{-y_4}{(x_1 - x_4)^2} \tag{13}$$

$$b = x_4 \tag{14}$$

$$c = y_4 \tag{15}$$

Consistently with the real eye, the synthetic iris contour edges that lie between the upper and lower eyelids are located and used to fit the elliptical contour in our simulations. For instance, curves U_1L_1 and U_2L_2 shown in Fig. 4(b) are the fitting edges that we want. These fitting edges can be located by using the equations of iris and eyelids. We will investigate the performances of our method using the eye model of dimensions close to that for human in Section 3.1.2.

3.1.2. Performance study with synthetic data

Some factors motivate us to do simulations. The unit surface normal directions to the supporting planes of the two iris contours are parallel when the person focuses at infinity. They are nearly parallel when the focus distance is great. However, there is a noticeable angle when the focus distance is near. On the other hand, we cannot ideally predict an identical supporting plane, even the person focuses at infinity due to some factors including eyelid occlusion, inaccuracy of camera calibration, and image processing. Hence, we are seeking the unique supporting planes that have the minimal difference in normal directions, as stated in the 'normal direction constraint'. We will show (by simulation) that we can disambiguate the solutions of the normal to the supporting plane considering these factors. We can also see the accuracy and robustness of our algorithm.

The dimension in the simulation is as close as real statistical data of human eye. The intrinsic parameters of a camera (gaze camera) are set approximately same with the real parameters of the real camera. The centers and the radii of the two irises are set approximately same with the real statistical dimension of human face. The coordinate system of the camera is defined as above, i.e. the image plane is defined as the X–Y (X — horizontal axis, Y — vertical axis) plane and the Z-axis is along the optical axis of the camera and pointing towards the frontal object. Two irises are initially positioned parallel to the X–Y plane of the camera and symmetrical about Y–Z plane of the camera coordinate system. In order to mimic the iris movements, we define 'rotation center' for the two irises, about which the iris will rotate making the gaze lines merge at indicated focus

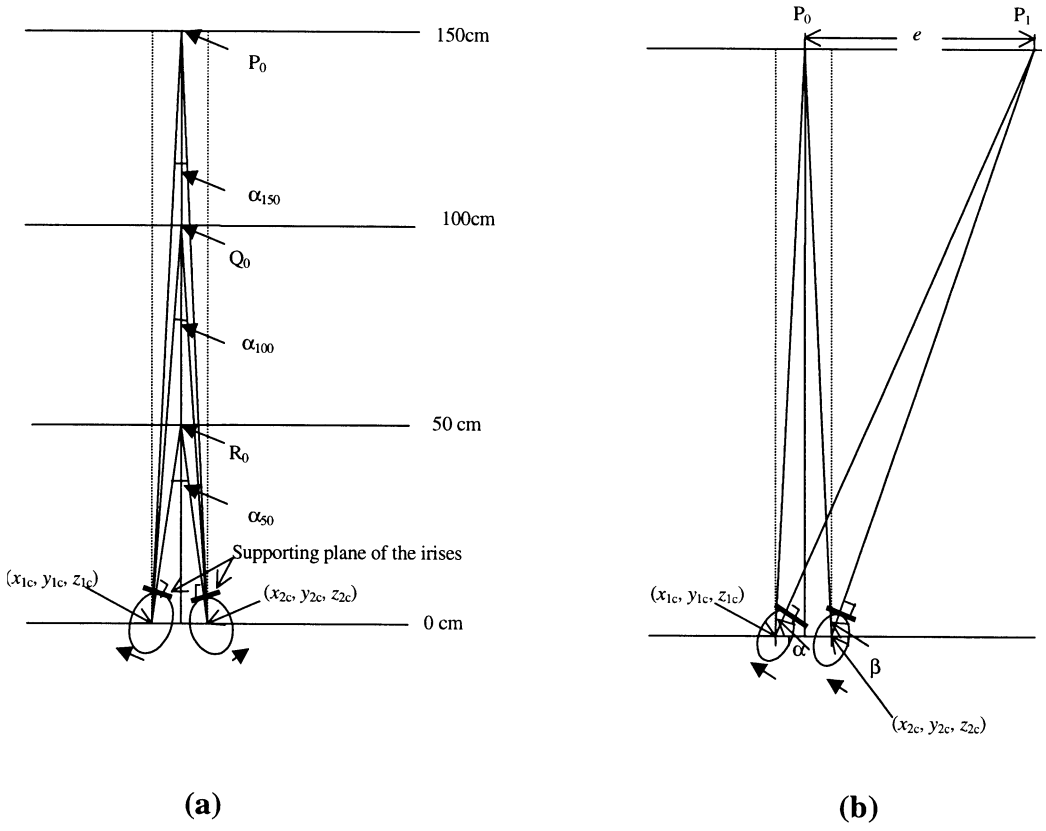

Fig. 5. Two sets of simulation, (a) the errors versus the vergence movements, the movement of the two eyeballs are in the opposite direction, (b) the errors versus the smooth pursuit movements, the movement of the two eyeballs are in the same direction.

point. Extending the initial normal to the supporting plane of the iris a 'eyeball's radius' toward inner of the eye. The 'eyeball's radius' is a constant in proportion to the iris's radius. We have stated that the angle between the gaze (center line of the eyeball) we defined and the true gaze is fixed. Without loss of generality, we consider the center line of the eyeball as the true gaze in our simulations.

The projective image can be obtained using the perspective transform matrix of the camera. The two projective ellipses can be fitted. The 3D location (six degrees of freedom, three for translation and three for rotation) can be calculated using Eqs. (5) and (8). Hence, the errors between the calculated results and corresponding original synthetic data were obtained. We test the errors under different poses. An example is given as follows.

The size of the image is 640×480. The intrinsic parameters of the camera are set as follows.

$$u_0 = 320 \tag{16}$$

$$v_0 = 240 \tag{17}$$

$$f_x = f_y = 3500 \tag{18}$$

where (u_0, v_0) are coordinates of the principal point, the scale factors of the camera along the x- and y-axis, f_x and f_y, respectively, are set according to our measurements using real camera (zoom-in) in order to produce high-resolution iris images. A 40–45 mm lens is used in our real image experiments while keeping the camera at a distance of about 0.5 m to the human face. The 3D coordinate (with respect to the coordinate system of camera) of the centers of the two iris contours (named as iris-1 and iris-2) given in cm, are:

$$(x_{1c}, y_{1c}, z_{1c}) = (-3.25, 0, 60) \tag{19}$$

and

$$(x_{2c}, y_{2c}, z_{2c}) = (3.25, 0, 60) \tag{20}$$

i.e. the camera is initially put at a distance 60 cm to the human face and two iris contours (circles) lie parallel to the image plane, see Fig. 5. The radii of the two irises are same:

$$r_1 = r_2 = 0.65 \text{ cm} \tag{21}$$

The distance between two extreme corners of the parabola, see Fig. 4, is assumed:

$$P_1P_3 = 3.5 \text{ cm} \tag{22}$$

The top and bottom points of parabola are symmetric about the initial iris center, see Fig. 4, the distance:

$$P_2O = P_4O = 0.6 \text{ cm} \tag{23}$$

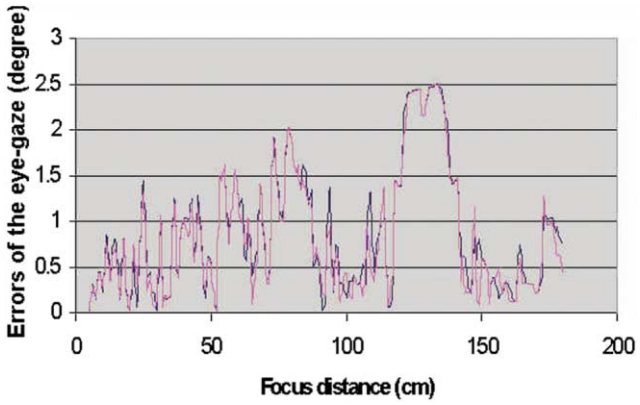

Fig. 6. The errors (absolute) of the eye-gaze (iris-1: dark, iris-2: light) versus the focus distances.

Two types of eye movements are considered in our simulations: vergence movements and smooth pursuit movements [33]. The primary difference between the two eye movements is that binocular pursuit movements are conjugate (moving in the same direction in both eyes, see Fig. 5(b)), whereas vergence movements are disconjugate (moving in different directions, see Fig. 5(a)).

3.1.2.1. Experiment 1: vergence eye movements We measure the performance of the 'normal direction constraint' when the vergence movements of the eye occur, see Fig. 5(a). It is noticed that the schematic dimension is not scaled as the real dimension in Fig. 5. The supporting planes of the two iris contours are rotated around their 'rotation center', respectively, so the two eye-gaze line meet at the focus point. The gaze errors are measured for varying focus distance. At a focus distance, two eye-gaze lines meet at the focus point. In our simulation, once the focus point is fixed, connecting the centers of the two irises with the focus point, respectively, forms the gazes of the two eyes. The supporting planes of the two irises are thus located once their normal directions, i.e. gaze, are fixed. The initial supporting planes of the two irises are rotated, respectively, about their 'rotation center' to reach the

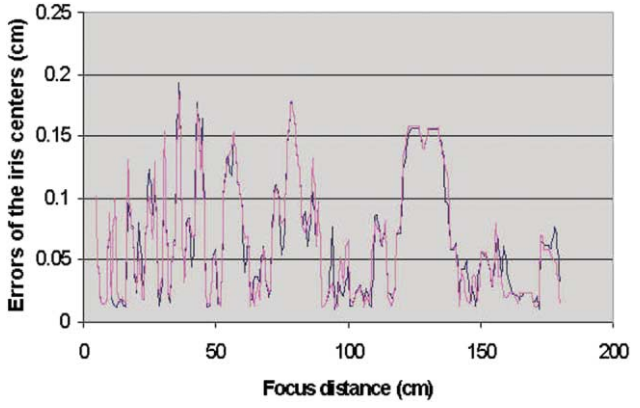

Fig. 7. The errors (absolute) of the irises' centers (iris-1: dark, iris-2: light) versus the focus distances.

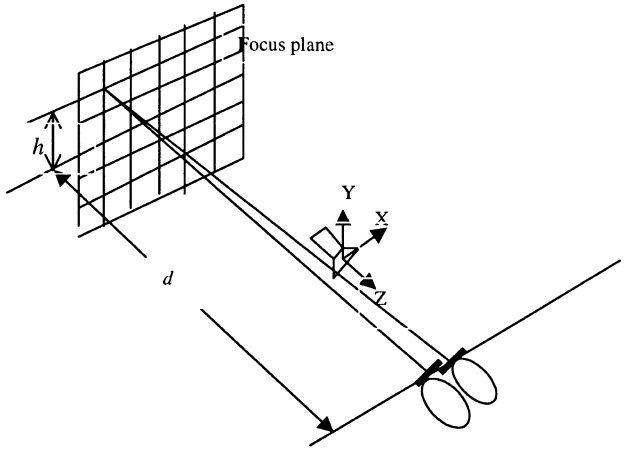

(a)

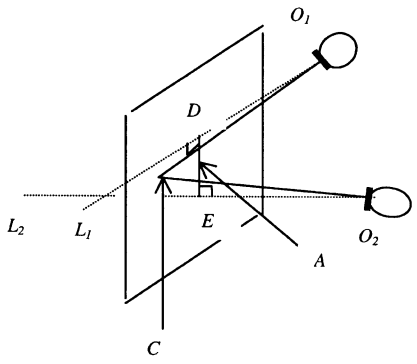

(b)

Fig. 8. Experiments on the accuracy of the eye-gaze versus the focus points, (a) a person observes the grid; a camera is put in front of the person; the gaze of the two eyes can be determined using the image of the irises, (b) the mid-point (A) of the segment (DE), which is the shortest distance between the estimated gaze of the two eyes (O_1L_1 and O_2L_2), is taken as the estimated focus point; O_1C and O_2C are the true gaze of the two eyes.

normal direction. The normal to the supporting planes and the iris's centers can be estimated from the projection of the contours of the two irises via 'two-circles' algorithm. The error can be obtained by comparing the results with the true pose. The angle between the two eye-gaze lines is:

$$\alpha = \tan^{-1}(2d/(L/2)) \tag{24}$$

where d is the distance between the focus point and line passing through the 'rotation center' (horizontal) of the two irises. L is the distance between the 'rotation center' of the two irises.

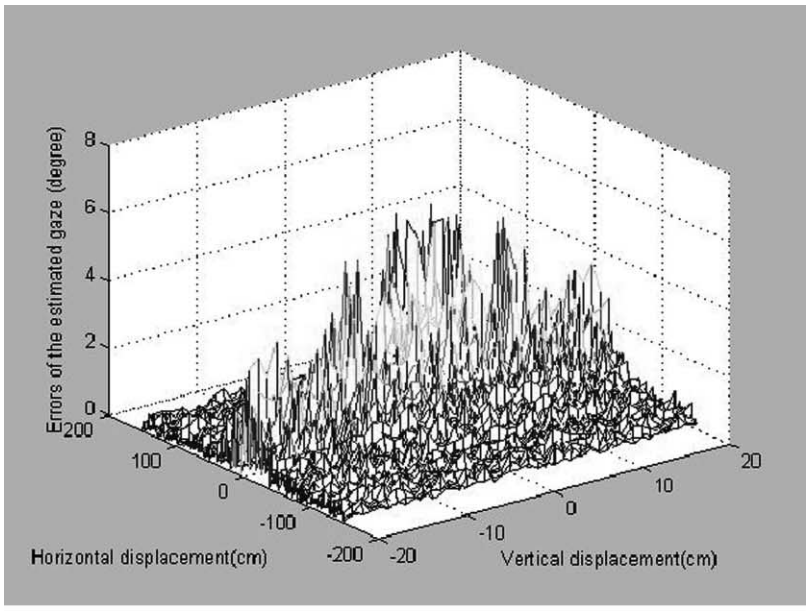

(a)

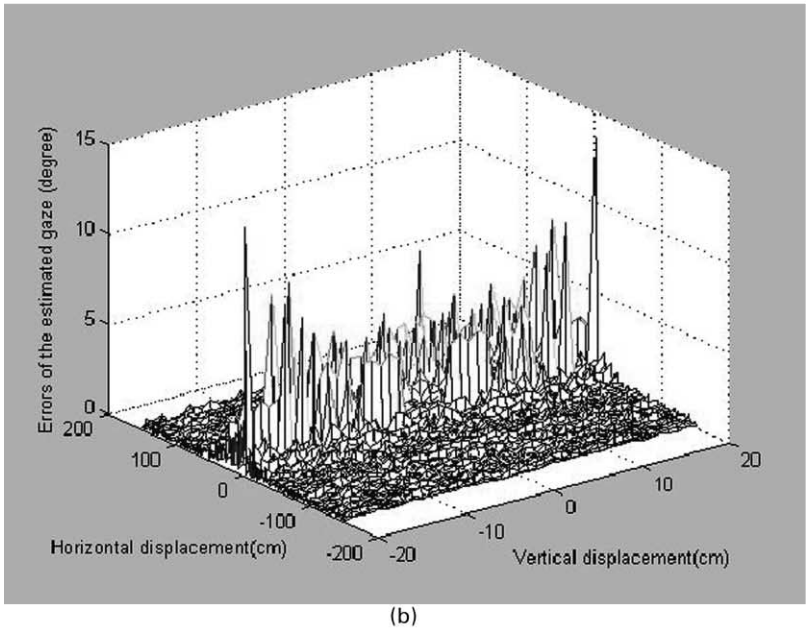

(b)

Fig. 9. The errors of the gaze versus the different focus points, the distance between the focus plane and the human face is 1.5 m, (a) left iris, (b) right iris.

From Eqs. (19) and (20), we know $L = 6.5$ cm.

The angles between the gaze of the two eyes are (when distances are 1.5, 1 and 0.5 m, respectively, see Fig. 5(a)):

$$\alpha_{150} = 2.48^\circ, \quad \alpha_{100} = 3.72^\circ, \quad \alpha_{50} = 7.44^\circ \tag{25}$$

The errors of the gaze and the iris centers are shown in Figs. 6 and 7, respectively.

3.1.2.2. Experiment 2: pursuit eye movements In this experiments, a focus point is moved on a plane, which has constant distance to the human face, see Fig. 8. Using the similar approach mentioned above, we located the supporting planes of the two irises such that the gaze of the two eyes met at the moving focus point. Then the errors of the eye-gaze are measured using 'two-circles' algorithm. The focus point moves in vertical axis from -20 to 20 cm in steps of 1 cm (azimuth) and in horizontal axis from -150 to 150 cm in steps of 1 cm (elevation) forms a set of synthetic images. The gaze errors are shown in Fig. 9, the errors of the iris center are shown in Fig. 10 where the distance between the focus plane and the human face is 1.5 m. The focus point moves on the grid point from

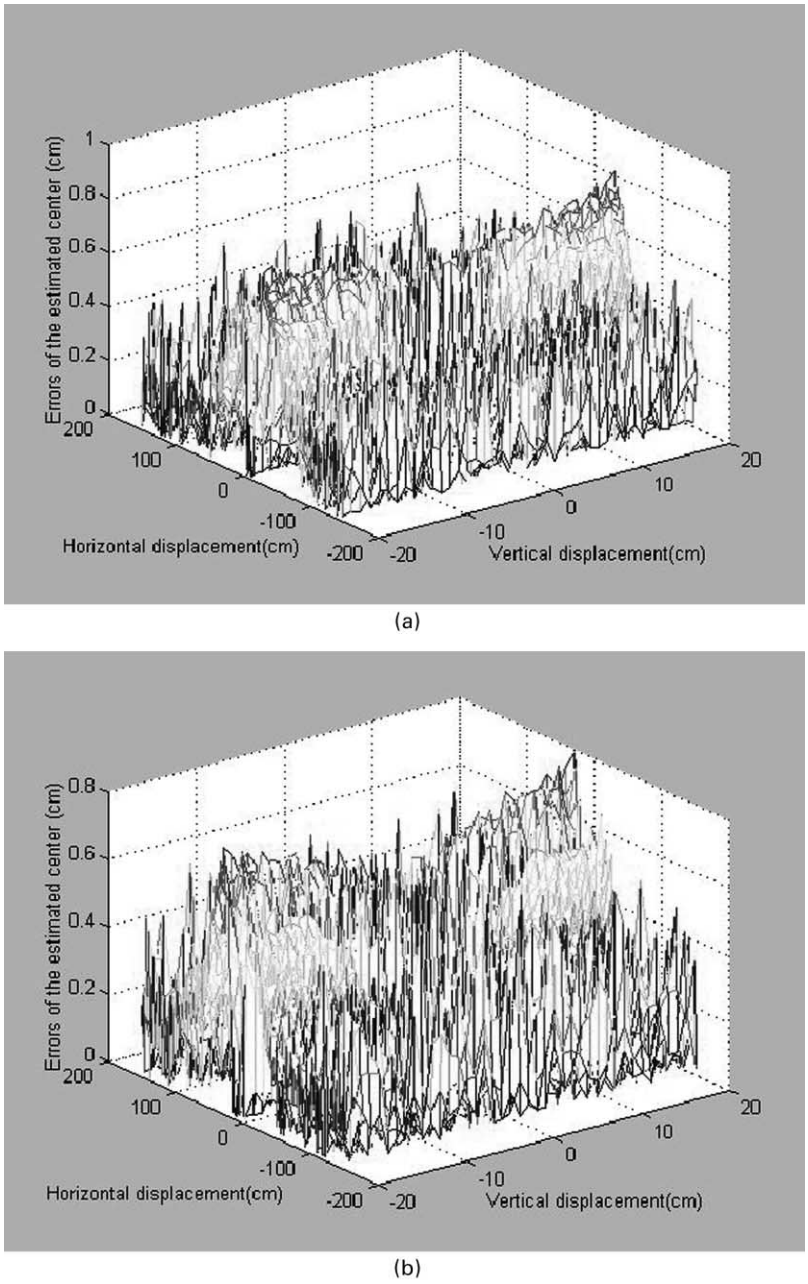

Fig. 10. The errors of the iris center versus the focus points, distance between the focus plane and human face is 1.5 m, (a) the left iris, (b) the right iris.

bottom to top, left to right. We can see that the largest errors occur when the focus object lies at the exact fronto-parallel position.

In order to rotate the contours of the two irises meeting at the focus point, we need to calculate the rotation angle with respect to the initial position of the contours. We can calculate the angle between the gaze of the two eyes and the initial iris plane as follows, see Fig. 5(b).

```
if (e < x_1c)
  {
  α = −atan((x_1c − e)/d);
  β_1 = −atan((x_2c − e)/d);
  }
else if ((e > = x_1c) && (e < x_2c))
  {
  α = atan((−x_1c + e)/d);
  β_1 = −atan((−e + x_2c)/d);
  }
else
  {
  α = atan((−x_1c + e)/d);
  β_1 = atan((e − x_2c)/d);
  }
```

where e is the displacement of the focus point away the

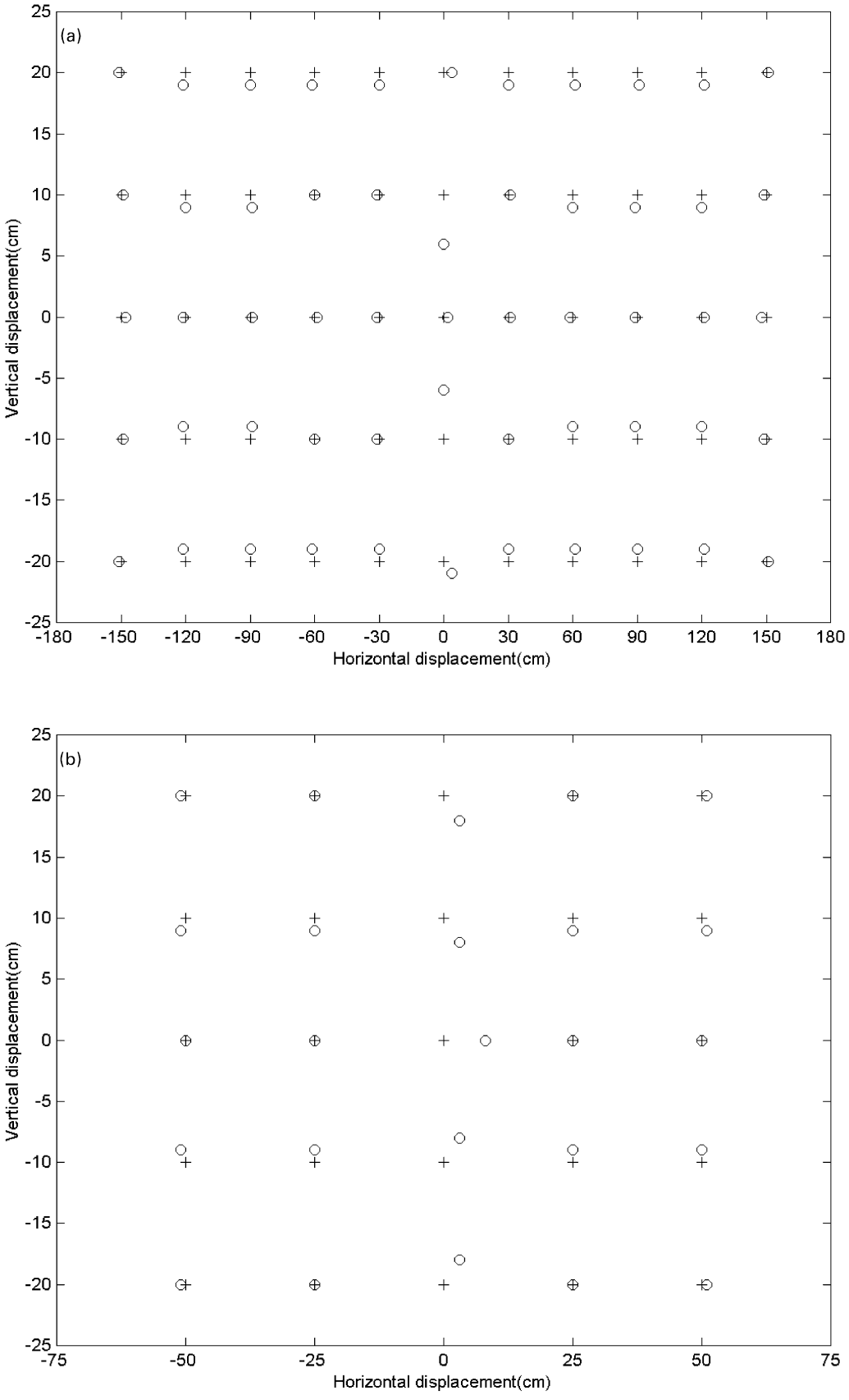

Fig. 11. The errors of the estimated focus points, the points marked '*' are the true focus points and the points marked 'O' are the estimated focus points. The distance between the focus plane and human face is, (a) 1.5 m, (b) 1.0 m, (c) 0.5m.

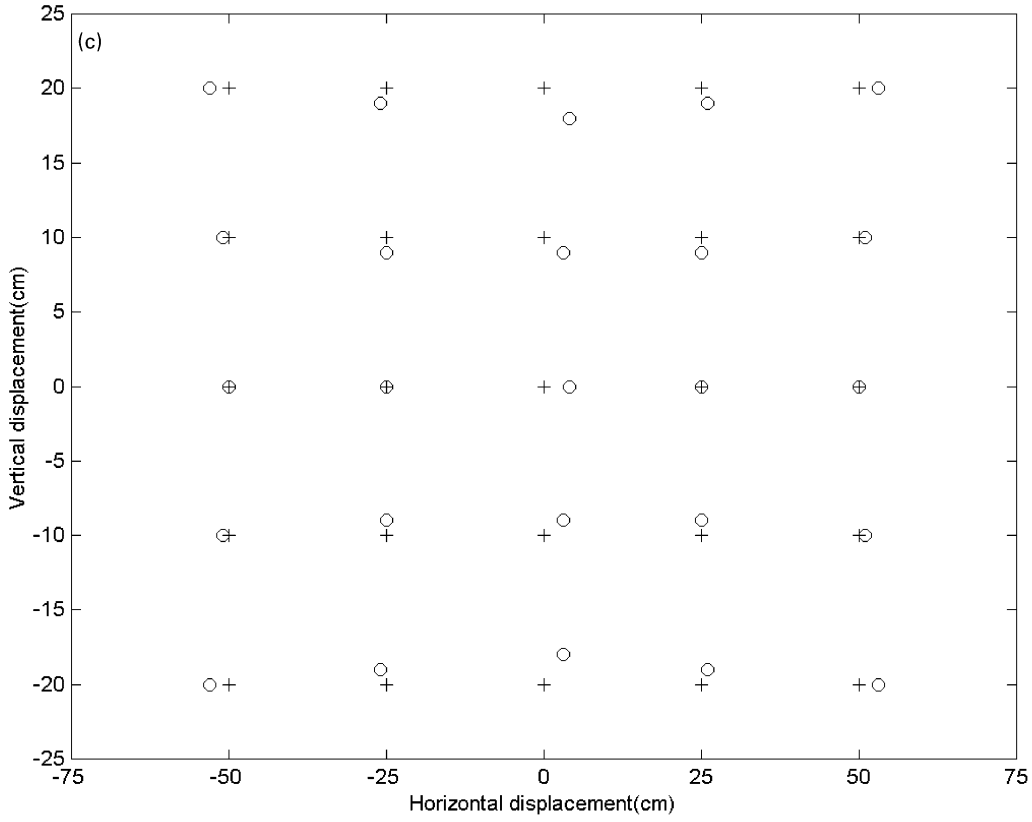

Fig. 11. (*continued*)

exact fronto-parallel, d is the distance between the focus plane and the human face.

Considering the focus point moving in the vertical orientation, the rotation angle of the normal to the supporting plane of the two irises should be as follows

```
if (e < x2c)
{
   α = −atan(h/sqrt(d^2 + (−x1c + e)^2));
   β_1 = −atan(h/sqrt(d^2 + (x2c − e)^2));
}
else
{
   α = −atan(h/sqrt(d^2 + (−x1c + e)^2));
   β_1 = −atan(h/sqrt(d^2 + (e − x2c)^2));
}
```

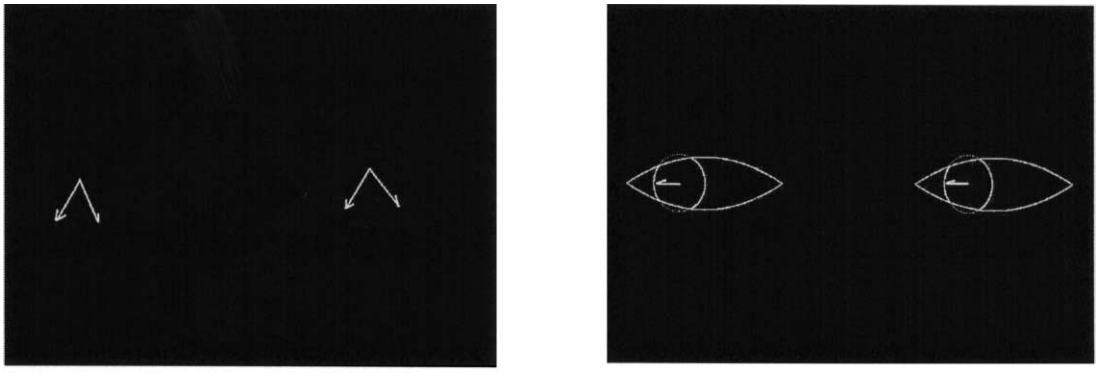

(a) (b)

Fig. 12. Disambiguation of the normal shown in Table 2. (a) The normal solutions of the two eyes (top view), (b) The edges of the irises, the fitted ellipses and the estimated gaze.

Table 1
The results of the normal of the two circles

	Solution-1	Solution-2
Circle-1		
Gaze	(−0.5102, −0.0007, 0.8600)	(0.3971, 0.0005, 0.9178)
Center	(−3.8128, −0.0086, 59.9364)	(−3.8185, −0.0087, 59.9361)
Circle-2		
Gaze	(−0.5438, −0.0001, 0.8392)	(0.6162, −0.0001, 0.7876)
Center	(2.6578, −0.0085, 59.6596)	(2.6511, −0.0085, 59.6599)

where h is the displacement of the focus point in the vertical axis, see Fig. 8 (a).

In Fig. 9 we can see that the error is largest in the frontal parallel position. The error is lower than 1° when the focus point is 30 cm away from the fronto-parallel position while the focus distance is 1.5 m. In our application the larger errors, which occurred near fronto-parallel positions, can be prevented by putting the camera at a slight skew angle about 10°.

3.1.2.3. Experiment 3: accuracy of the estimated focus points In order to test the displacement of the estimated focus points, we calculate the focus point using the gaze of the two eyes obtained using 'two circles' algorithm. The gaze of the two eyes computed using "two-circles" algorithm are generally not coplanar due to the noise, i.e. the shortest between the two lines is not zero. We take the mid-point of the segment, which is the shortest distance between the gaze of the two eyes, as the estimated focus point. This can be seen in Fig. 8(b). Assuming that O_1 and O_2 are the centers of the two contours of the irises; lines O_1C and O_2C are the true gaze of the two eyes, respectively. The dot-lines of O_1L_1 and O_2L_2 are the estimated gaze of the two eyes where DE is the common perpendicular line of the O_1D and O_2E. The mid-point of the DE is at A, the estimated focus point. In Fig. 11, we show the errors of the focus points, where the points marked ' + ' are the true focus points and the points marked 'O' are the estimated focus points. In this experiment, the mid-point of the two center of the iris and the mid point of the estimated focus points are connected as the average gaze. The focus point marked 'O' is the intersection point of the gaze and the focus plane. It is shown that the largest error occurs when the eyes focus at the exact fronto-parallel object point.

We discuss the accuracy in details using an example. Assuming that a focus point is at focus plane distance 1.5 m, point away from the fronto-parallel view 93 cm, no displacement in the vertical direction. The projection of the two iris contours is shown in Fig. 12. The results of normal vectors (gaze) and centers of circle-1 (left) and circle-2 (right) are listed in Table 1.

Using the symbolic definition in Section 2.2.2, the angle between n_{11} and n_{21}, n_{11} and n_{22}, n_{12} and n_{21}, n_{12} and n_{22} are 2.266, 68.720, 56.340, and 14.646°, respectively. So, n_{11} and n_{21} are the solutions based on our 'normal direction constraint'. The errors of the gaze of the two eyes are 0.218 and 0.259°, respectively. The unit normal directions (listed in Table 1) to the two iris contours are shown in Fig. 12, where the solution of a normal direction of an iris is drawn as a unit vector starting from resulting iris's center. The double arrow line (corresponding to n_{11} and n_{21}, respectively) is obviously the unique solution of the two irises, compared with the single arrow lines (corresponding to n_{12} and n_{22}, respectively), based on our 'normal direction constraint'.

The centers of two circles are calculated using formula (8) and errors are listed in Table 2.

We will test the robustness of the algorithm to geometrical disturbances in Section 3.2.

3.2. Robustness to geometrical disturbances

We test the robustness of our algorithm by testing the errors caused by geometrical disturbances.

Using the virtual camera and two irises assumed in Section 3.1.2. the locations of the imaged features were corrupted by zero-mean standard Gaussian noise. The errors of the gaze vectors and the centers of the iris contours are measured on the noised image.

Once a pose is given, we disturbed the image coordinate of the feature points using Gaussian noise and estimated the errors, both of the gaze and the center of the contours. We do this kind of simulation 100 times at the pose and take the mean error of them. The results when the positions of fitting points are perturbed by a standard Gaussian noise (mean zero, standard deviation is one pixel) are shown in Fig. 13 (gaze) and Fig. 14 (center of the irises). The errors of the focus points are shown in Fig. 15.

The experiments show that the algorithm we developed is robust enough. When we disturb 2D positions of iris contour fitting points with a standard Gaussian noise, the errors of the gaze of different poses are less than 2°, the error of the centers of two circles are both less than 0.15 cm.

Table 2
The errors of the centers of the two circles

	Calculated (cm)	Real (cm)	Error (cm)
Circle-1	(−3.8128, −0.0086, 59.9364)	(−3.7982, 0, 59.8485)	0.0895
Circle-2	(2.6578,−0.0085, 59.6596)	(2.6734, 0, 59.8309)	0.1722

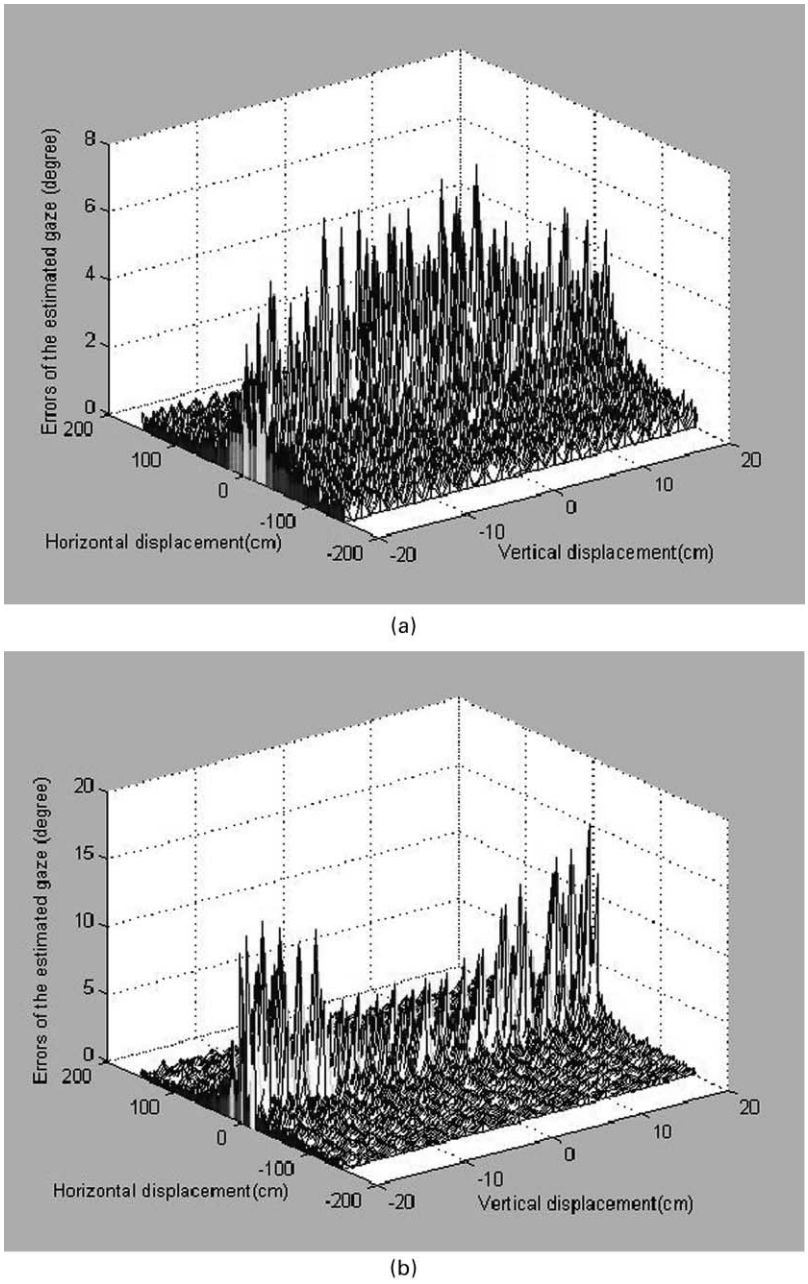

Fig. 13. The errors of the eye-gaze is shown when the focus points move in a plane away 1.5 m, the position of the point are disturbed by the standard Gaussian noise (mean zero, standard derivation one pixel), (a) the left iris, (b) the right iris.

3.3. Experiments on real scene

We have done some experiments using the real face images to evaluate our gaze estimation approach. The experiments include different persons (the radii of the different persons could have a little difference, so a calibration is needed), different lens, varying distance, etc.

The straight way to measure the accuracy of the algorithm is to compare the true focus points and the corresponding estimated focus points in space. Based on the discussions mentioned above about our approach, the camera should be put as close to the person as possible (high resolution) whereas the object should be put away from the person by about 1 m (see 'normal direction constraint'). So, we designed an experimental environment where a person can observe an object that is put behind the camera.

The detection of the iris has been discussed in Section 2.1. The processing can be executed within the eye region that is located by the pose determination [26]. In Fig. 16, we have shown an example for explaining the iris detection techniques that we have developed.

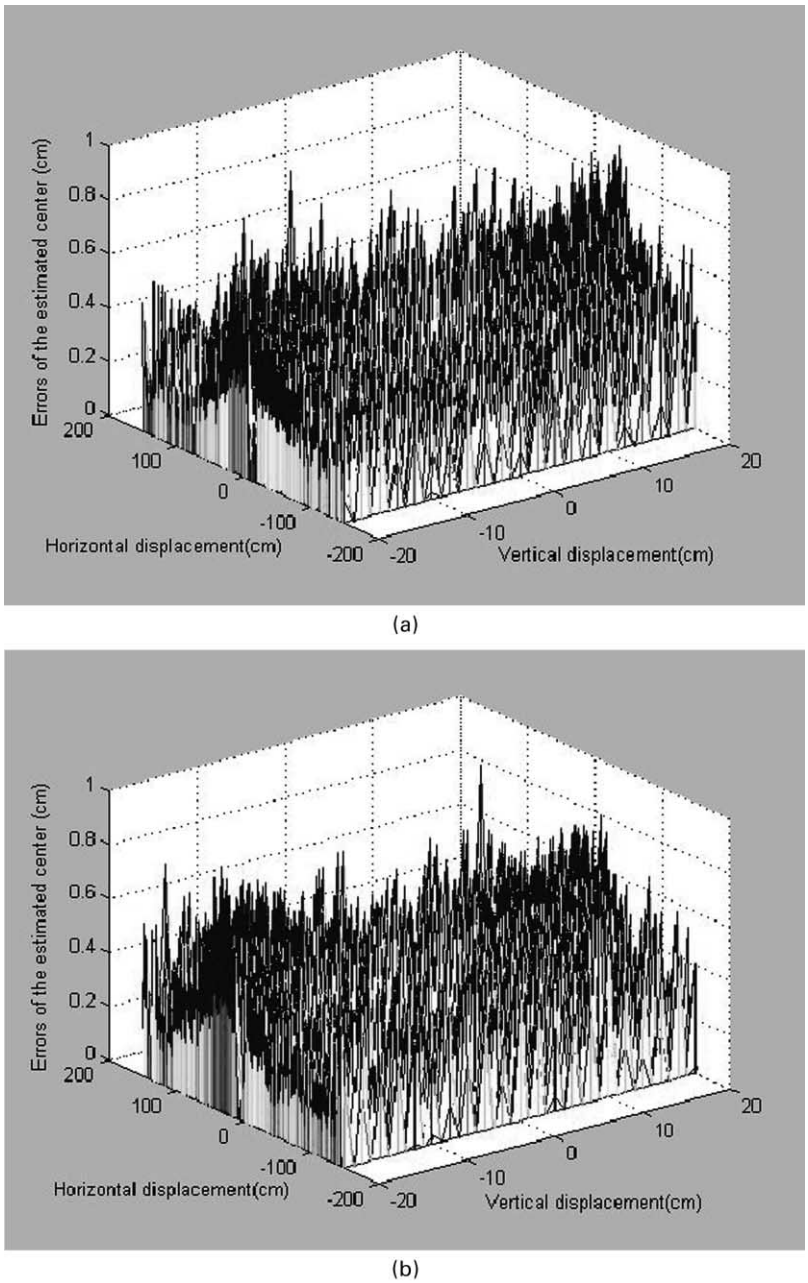

Fig. 14. The errors of the iris center versus the focus points, distance between the focus plane and human face is 1.5 m, the position of the point are disturbed by the standard Gaussian noise (mean zero, standard derivation one pixel), (a) the left iris, (b) the right iris.

We will discuss the experiments on focus point estimation as follows.

A camera with lens 45 mm is put in front of a person (nearly fronto-parallel) and away from the person about 1 m. The person observes an object (Philips monitor, screen size $40 \times 29\ \text{cm}^2$) that is behind the left of the camera. The distance between the object and the person is about 1.2 m. We put the object of interest in a fixed position in the world system where the gaze camera is calibrated. So we know the coordinate of the corners of the monitor with respect to the camera, we take these relative coordinates as the reference coordinate of the true focus points. The four images, where the person is observing the corners of the monitor in order, are captured. Consequently, the gaze corners of the monitors (focus points) can be obtained from the images. Then an error can be estimated by comparing the estimated focus points and the corresponding reference coordinate as mentioned above. The gaze estimation results are shown in Fig. 17. The radius of the iris contour is about 0.63 cm.

There are 640×480 pixels in the image of the irises. The intrinsic parameters of our camera are calibrated:

$$u_0 = 324.94 \tag{26}$$

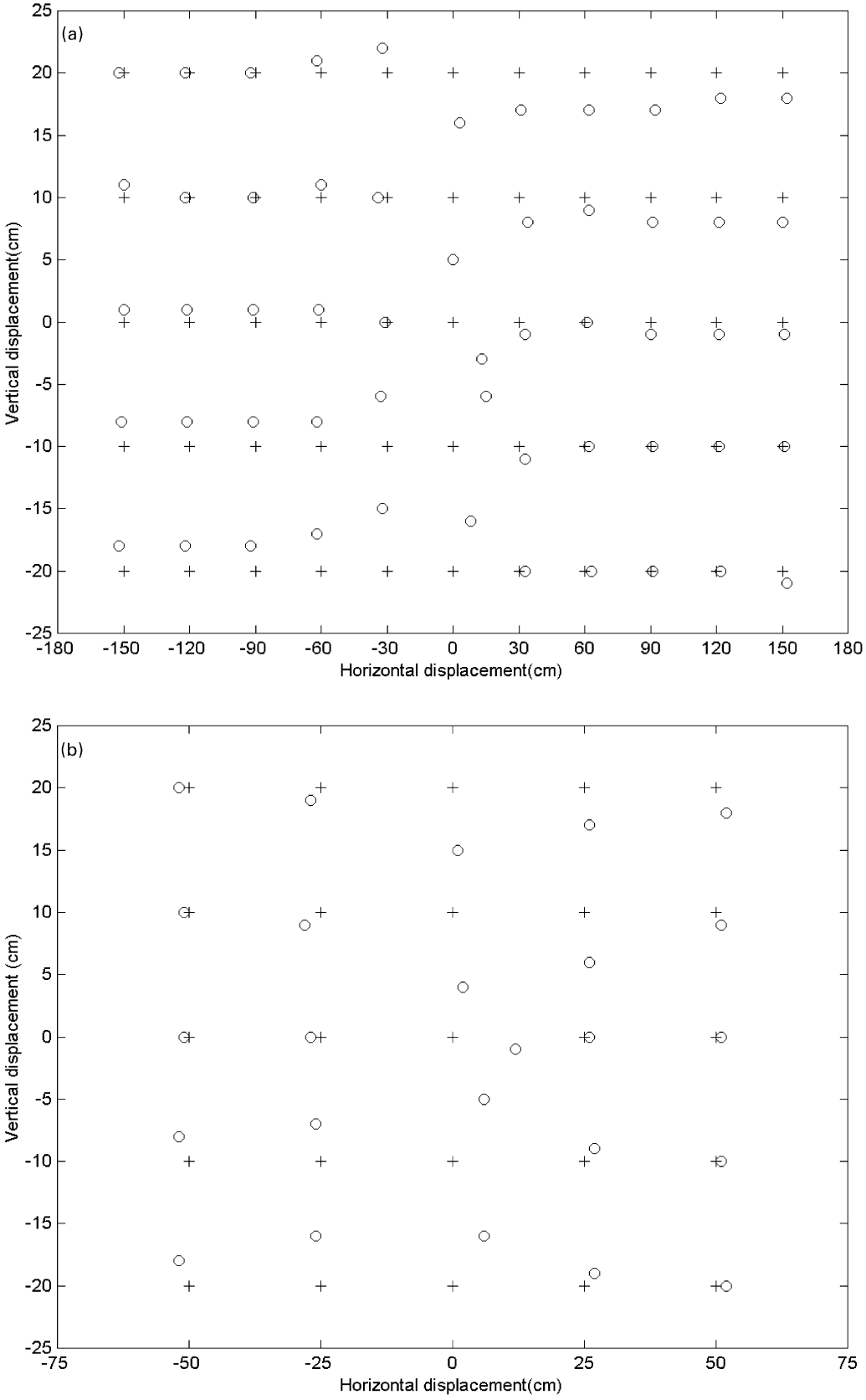

Fig. 15. The errors of the estimated focus points. The true positions of the points are disturbed by the standard Gaussian noise. The points marked ' + ' are the true focus points and the points marked '*O*' are the estimated focus points. The distance between the focus plane and human face is, (a) 1.5 m, (b) 1.0 m; (c) 0.5 m.

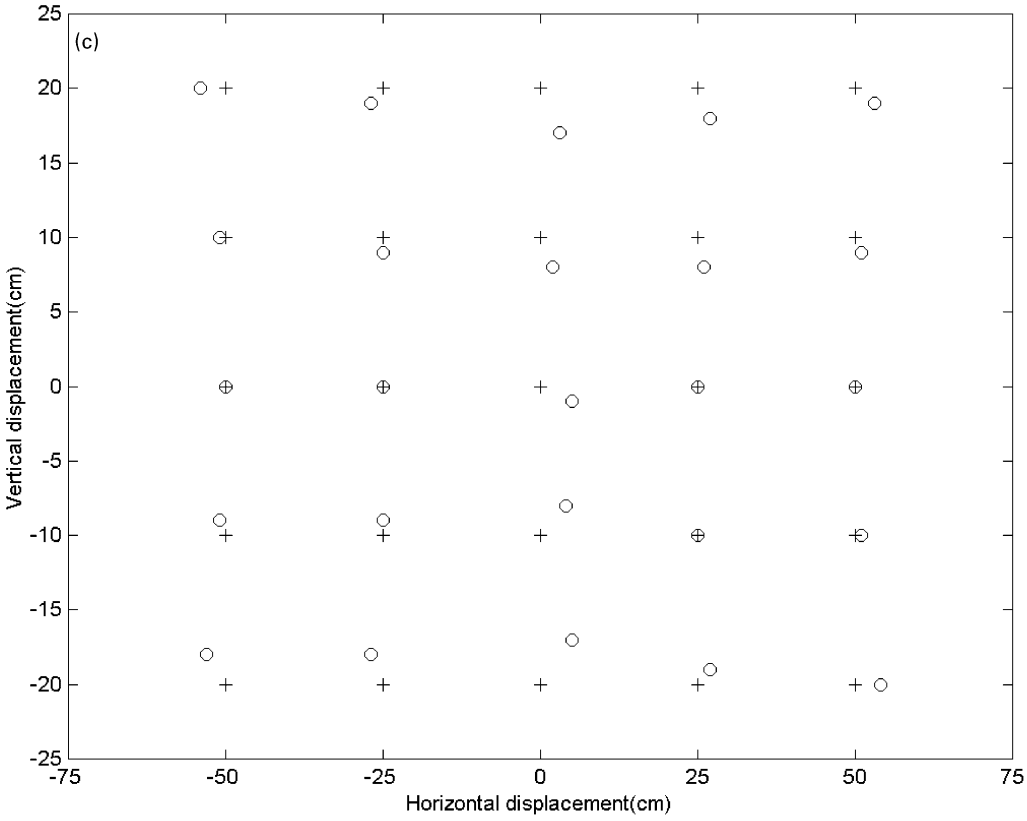

Fig. 15. (c) (*continued*)

$$v_0 = 247.97 \tag{27}$$

$$f_y = 3485.10 \tag{28}$$

$$f_y = 3671.49 \tag{29}$$

There are about 200 edge points for fitting left and right ellipses, respectively. The two solutions of the normal vector and the center of two ellipses are calculated. The results in detail are listed in Table 3.

The distance from the camera to the person is about 75 cm. This can be seen from the results of the centers of the irises in Table 3. The angle between the estimated gaze and the true gaze, a vector starting from the estimated center

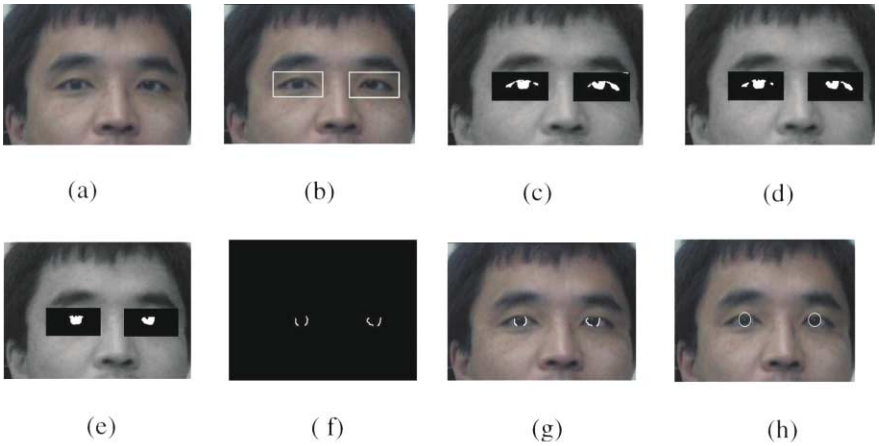

Fig. 16. Iris contour detection and gaze determination, (a) original image, (b) the eye-regions located by the pose determination method, (c) segmentation results of the eye-regions, (d) separating the irises using morphological open (2×2 structuring element)operation, (e) the largest segmented regions within the eye-region are deemed to be the irises, (f) the longest vertical edges (3×3 vertical operator) are deemed to be the irises edges, (g) overlaying the irises edges onto the original image, (h) overlaying the fitted ellipses onto the original image.

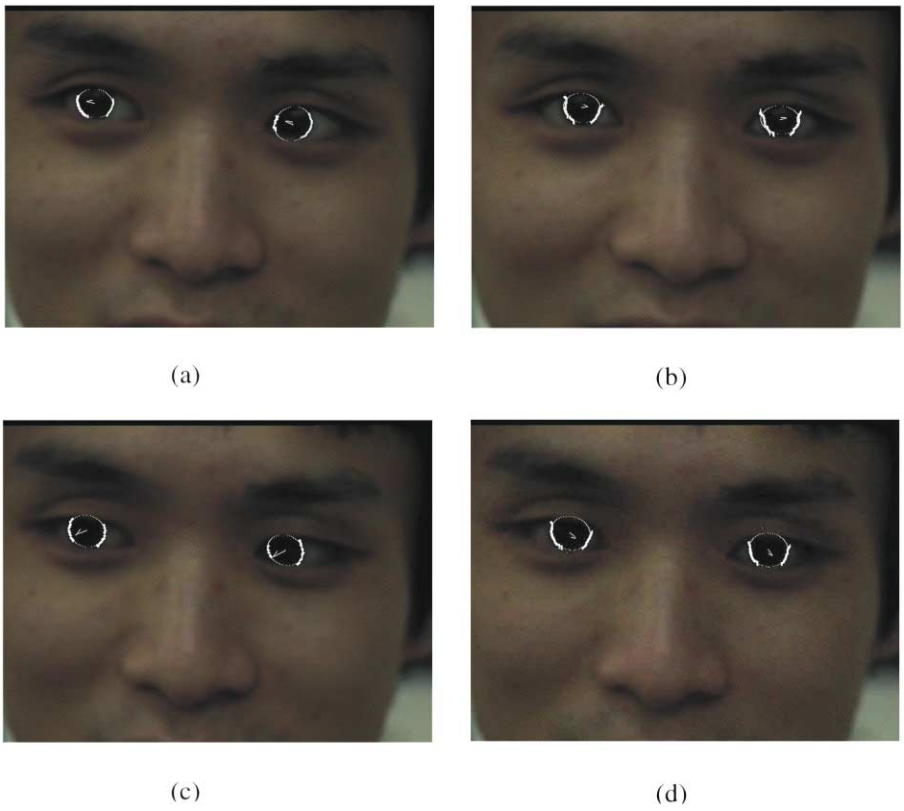

Fig. 17. The gaze when a person looks at the four corners of a monitor in order. The edges of the irises, fitted ellipse contours and the gaze are overlaid onto the original images, (a) upper-right, (b) upper-left, (c) bottom-right, (d) bottom-left.

of the iris to the reference points mentioned above, is taken as the error of the gaze. We can explain this using Fig. 8(b) where the angle between the O_1A and O_1C and the angle between O_2A and O_2C are the gaze errors of the left and right eye, respectively.

We have stated that we cannot expect the gaze of the two eyes intersecting at a point in space due to inaccurate camera calibration and image processing. The shortest distance between the gaze of the two eyes, used to locate the 'estimated focus points', are found to be quite small. In this experimental example, they are 0.30, 0.43, 0.01 and 0.11 cm, respectively, when the person observes the corners in order. This also shows that the gaze we defined in this paper is applicable to represent the attention of the human.

The errors are caused due to the image noise, morphological 'open' operation employed to detect the iris edges and camera calibration. However, it could also be caused mainly by the effect of the angle between the antimony gaze and the

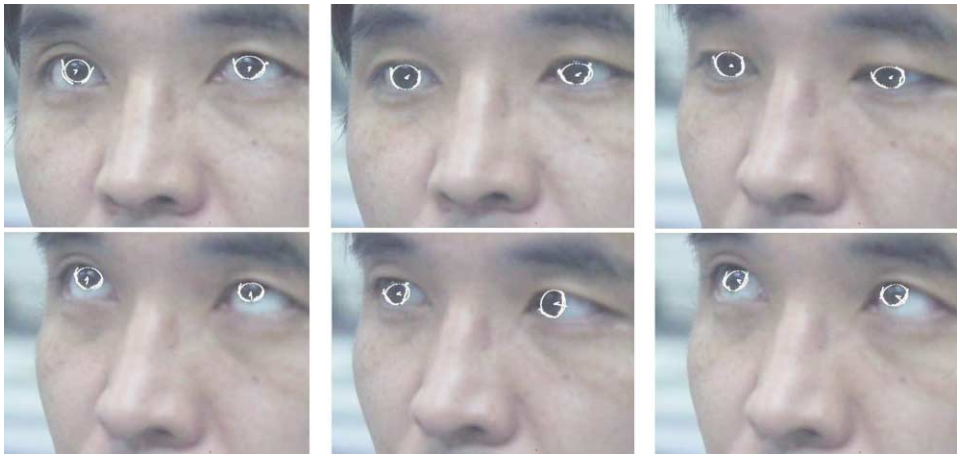

Fig. 18. Some examples of the eye-gaze determination results (overlaying the iris edges, fitted ellipses and the gaze directions onto the original images).

Table 3
Gaze determination and focus point estimation (Note: C: Center of the iris contour (cm); G: Gaze; E: Estimated focus point (cm); R: Reference focus point (cm); LE: error of the gaze of the left eye; RE: error of the gaze of the right eye.)

Pose	Left	Right	Focus points	Error
(d)	C: (−3.612607, −0.123945, 74.712240)	C: (2.923129, −0.128169, 74.856711)	E: (39.290848, 12.641216, −43.343605)	LE: 0.73^0
	G: (−0.339758, −0.099915, 0.935191)	G: (−0.292573, −0.103917, 0.950580)	R: (40, 14.5, −45)	RE: 0.64^0
(b)	C: (−3.612313, 0.102581, 74.705642)	C: (2.923148, 0.106827, 74.854271)	E: (38.745293, −12.524923, −41.832115)	LE: 0.75^0
	G: (0.339735, 0.099605, 0.935232)	G: (−0.292030, 0.104673, 0.950664)	R: (40, −14.5, −45)	RE: 0.69^0
(c)	C: (−3.856879, −0.096348, 74.567535)	C: (2.659401, −0.102780, 74.712286)	E: (76.769348, 11.460166, −39.991791)	LE: 1.02^0
	G: (−0.573595, −0.082166, 0.815008)	G: (−0.540747, − 0.084421, 0.836939)	R: (80, 14.5, −45)	RE: 1.02^0
(a)	C: (−3.857074, 0.074951, 74.569134)	C: (2.659461, 0.081426, 74.714108)	E: (76.332527, −11.337215, −39.321533)	LE: 1.00^0
	G: (−0.573778, 0.081283, 0.814968)	G: (−0.540752, 0.084195, 0.836958)	R: (80, −14.5, −45)	RE: 1.01^0

gaze we are defining. As discussed in Section 3.1.1, this is a matter of calibration.

We have tried our algorithm over 50 images. The results are satisfactory. Another set of gaze results of a different person is shown in Fig. 18. The radius of the iris contour is calibrated. We can see that the gaze results coincided well with the observations. The radius of the iris contour is calibrated, where we assume the radius of the two irises are both 0.65 cm and the 'rotation center' is assumed to be at a distance 1 cm to the supporting plane of the iris. These facial dimensions are of a person. The centers of the two irises can be calculated. In Fig. 18, the two arrows ending at the iris's centers, respectively, represent the eye-gazes.

4. Conclusion

In this paper, we present a non-invasive method for robustly estimating an adequate eye-gaze by iris imaging. This method is based on a simple 'two-circles' principle we proposed. This principle states that the orientation of a pair of parallel supporting planes can be uniquely deduced from an image of the two circles, each lying on one of the supporting planes. This principle is applied to the eye-gaze by observing that the contours of the two irises are circular and that they lie on parallel supporting planes when focused at infinity (hence, they are the two circles that we are looking for). However, the angle between the two eye-gaze-line is noticeable when the focus distance is near, so the 'normal direction constraint' we are using states that the difference of the normal to the supporting plane of the two irises should be minimal irrespective the eyeball and head rotation. The solutions of the gaze and the center of the iris contour in space can be disambiguated using this constraint. Others have never tried the use of iris contours in this way before.

Compared with the other approaches, the shape of the eye is not required in our approach; only the radius of the iris is needed. Consequently, the problem namely compensation of the head movements, necessary in other approach where the center of the eyeball is assumed, does not need to be considered. On the other hand, different from the existing eye models, iris contours are accurately modeled as two circles and we estimate the ellipses of their projections onto an image plane. The variances of the eccentricity of the fitted ellipses can verify our above assumption. Our gaze determination method combines iris detection and quadratic curve-based pose determination method effectively. The largest error of the gaze estimation of our approach occurs when the gaze orientation is nearly parallel to the optical axis of the camera. This case has been prevented in our application (human–machine interaction) by simply putting the camera on top of the monitor and slightly skewed to the face. The accuracy and robustness of this approach were verified by the experiments on synthetic and real image data. Simulations on a virtual camera models have shown that the algorithm is robust under geometric disturbances. When we disturb the 2D position of the points of the iris edges using a standard Gaussian noise, the error of the rotation angle is less than 2°, the error of the centers of the two irises is less than 0.2 cm within the range of 1.5 m.

A zoom-in camera is used to get high-resolution iris images. A general approach that combines head-pose determination with eye-gaze estimation is proposed. A second camera is used for the determination of the head-pose. The camera, which focuses on the irises using the head-pose information, provides sufficient resolution to measure accurately the rotation of eyeball.

Eye-gaze estimation is important in applications such as

virtual reality, video conferencing, human–machine interface/controls. The eye-gaze estimation method mentioned above, integrated with a head-pose estimation module together, will offer great potential especially in these applications. It is important to note that our method is non-invasive, fast and robust because the segmentation of the iris contours is one of the simplest and most robust facial features.

References

[1] A. Azarbayejani, T. Starner, B. Horowitz, A. Pentland, Visually controlled graphics, IEEE Transactions on PAMI 15 (6) (1993) 602–605.

[2] K. Kanatani, Analysis of Conics, Geometric computation for machine vision, Clarendon Press, Oxford, 1993 (chap. 8).

[3] C. Colombo, A.D. Bimbo, Interacting through eyes, Robotics and Autonomous Systems 19 (1997) 359–368.

[4] K. Talmi, J. Liu, Eye and gaze tracking for visually controlled interactive stereoscopic displays, Signal Processing: Image communication 14 (1999) 799–810.

[5] R. Herpers, M. Michaelis, K.H. Lichtenauer, G. Sommer, Edge and keypoint detection in facial regions, IEEE International Conference on Automatic Face and Gesture Recognition, 1996, pp. 212–217.

[6] D. Forsyth, J.L. Mundy, A. Zisserman, C.M. Brown, Projectively invariant representations using implicit algebraic curves, Image and Vision Computing 9 (2) (1991) 130–136.

[7] A. Gee, R. Cipolla, Determining the gaze of faces in images, Image and Vision Computing 12 (10) (1994) 639–647.

[8] R.M. Haralick, L.G. Shapiro, Computer and robot vision, Chapter 13. Perspective Projection Geometry, Addison-Wesley Publishing Company, 1993 (Chapter 13).

[9] T.E. Hutchinson, K.P.J. White, W.N. Martin, K.C. Reichert, L.A. Frey, Human-computer interaction using eye-gaze input, IEEE Transactions on System, Man and Cybernetics 19 (6) (1989) 1527–1533.

[10] X. Xie, R. Sudhakar, H. Azhang, On improving eye feature extraction using deformable templates, Pattern Recognition 17 (1994) 791–799.

[11] J.Y. Deng, F. Lai, Region-based template deformation and masking for eye-feature extraction and description, Pattern Recognition 30 (3) (1997) 403–419.

[12] R. Safaee-Rad, I. Tchoukanov, K.C. Smith, B. Benhabib, Three-dimensional location of circular features for machine vision, IEEE Transactions on Robotics and Automation 8 (5) (1992) 624–640.

[13] J. Porill, Fitting ellipses and predicting confidence envelopes using a bias corrected Kalman filter, Image and Vision Computing 8 (1) (1990) 37–41.

[14] Y.C. Shiu, S. Ahmad, 3D location of circular and spherical features by monocular model based vision, IEEE International Conference on System, Man and Cybernetics, 1989, pp. 576–581.

[15] R. Stiefelhagen, J. Yang, A. model-based, gaze tracking system, International Journal of Artificial Intelligence Tools 6 (2) (1997) 193–209.

[16] J.G. Daugman, High confidence visual recognition of persons by a test of statistical independence, IEEE Transactions on PAMI 15 (11) (1993) 1148–1161.

[17] J.G. Wang, Y.M. Hao, H.K. Cao, X.P. Xu, A visual navigation system for autonomous underwater vehicle, MVA'94 IAPR Workshop on Machine Vision Applications, Kawasaki, December 13–15, 1994, pp. 544–547.

[18] A. Zelinsky, J. Heinzmann, A novel visual interface for human-robot communication, Advanced Robotics 11 (8) (1998) 827–852.

[19] K.M. Lam, H. Yan, Locating and extracting the eye in human face images, Pattern Recognition 29 (5) (1996) 771–779.

[20] C. Colombo, A.D. Bimbo, Real-time head tracking from the deformation of eye contours using a piecewise affine camera, Pattern Recognition Letters 20 (1999) 721–730.

[21] A.L. Yulle, P.W. Hallnan, D.S. Cohen, Feature extraction from faces using deformable templates, International Journal of Computer Vision 8 (2) (1992) 99–111.

[22] S. Pastoor, J. Liu, S. Renault, An experimental multimedia system allowing 3-D visualization and eye-controlled interaction without user-worn devices, IEEE Transactions on Multimedia 1 (1) (1999) 41–52.

[23] D. Forsyth, J.L. Mundy, A. Zisserman, C. Coelho, A. Heller, C. Rothwell, Invariant descriptors for 3-D object recognition and pose, IEEE Transactions on PAMI 13 (10) (1991) 971–991.

[24] Q. Ji, M.S. Costa, R.M. Haralick, L.G. Shapiro, An integrated linear technique for pose estimation from different geometric features, International Journal of Pattern Recognition and Artificial Intelligence 13 (5) (1999) 705–733.

[25] M.D. Dhome, J.T. Lapreste, G. Rives, M. Richetin, Spatial localization of modeled objects of revolution in monocular perspective vision, 1st ECCV, 1989, pp. 415-485.

[26] J.G. Wang, E. Sung, Pose determination of human faces by using vanishing points, Pattern Recognition, submitted for publication.

[27] C. Colombo, A.D. Bimbo, S.D Magistris, Interfacing through visual pointers, in: R. Cipolla, A. Pentland (Eds.), Computer Vision for Human– Machine interaction, Cambridge University Press, 1998, pp. 135–153.

[28] S.D. Ma, Conics-based stereo, motion estimation, and pose determination, International Journal of Computer Vision 10 (1) (1993) 7–25.

[29] H.S. Sawhney, J. Oliensis, A.R. Hanson, Description and reconstruction from image trajectories of rotational motion, IEEE International Conference on Computer Vision 1995, pp. 494-498.

[30] H.H. Emsley, Visual Optics, 3rd ed., Butterworths, Scarborough, Ontario, 1955, p. 346.

[31] R. Cipolla, N. Hollinghurst, Visually guided grasping in unstructured environments, Robotics and Autonomous Systems 19 (3–4) (1997) 337–346.

[32] B. Allotta, C. Colombo, On the use of linear camera–object interaction models in visual serving, IEEE Transactions on Robotics and Automation 15 (2) (1999) 350–357.

[33] S.E. Palmer, Vision Science — Photons to Phenomenology, Visual selection: eye movements and attention, The MIT Press, Cambridge, Massachusetts, 1999 (Chapter 11).

[34] F.L. Bookstein, Fitting conic sections to scattered data, Computer Graphics and Image Processing 9 (1979) 56–71.

[35] R.M. Taylor, P.J. Probert, Range finding and feature extraction by segmentation of images for mobile robot navigation, Proceedings of the IEEE International Conference on Robotics and Automation, Minneapolis, Minnesota, April 1996, pp. 95–100.

[36] J.G. Wang, Head-Pose and Eye-Gaze Determination for Human–Machine Interaction, Ph.D. Thesis, Nanyang Technological University, School of Electrical and Electronic Engineering, Singapore, 2000.